

**Discrete Classification with Principal Component Analysis:
Discrimination of Giant and Dwarf Spectra in K-stars**

Rodrigo A. Ibata

Department of Physics and Astronomy, University of British Columbia,
2219 Main Mall, Vancouver, B.C., V6T 1Z4, Canada

Electronic mail: ibata@astro.ubc.ca

Michael J. Irwin

Royal Greenwich Observatory, Madingley Rd, Cambridge CB3 0EZ

Electronic mail: mike@ast.cam.ac.uk

Received _____; accepted _____

Submitted to The Astronomical Journal

ABSTRACT

We demonstrate the use of a variant of Principal Component Analysis (PCA) for discrimination problems in astronomy. This variant of PCA is shown to provide the best linear discrimination between data classes. As a test case, we present the problem of discrimination between K giant and K dwarf stars from intermediate resolution spectra near the Mg ‘b’ feature. The discrimination procedure is trained on a set of 24 standard K giants and 24 standard K dwarfs, and then used to perform giant – dwarf classification on a sample of ≈ 1500 field K stars of unknown luminosity class which were initially classified visually. For the highest S/N spectra, the automated classification agrees very well (at the 90 – 95% level) with the visual classification. Most importantly, however, the automated method is found to classify stars in a repeatable fashion, and, according to numerical experiments, is very robust to signal to noise (S/N) degradation.

Subject headings: Numerical techniques, stellar classification, K stars

1. Introduction

Studies of the large scale kinematic and chemical structure of our Galaxy often investigate the properties of samples of stars that are believed to trace Galactic mass. One of the most used species is the K giant (e.g., Ibata & Gilmore 1995a, Rich 1990, Rich 1988, Kuijken & Gilmore 1989, Lewis & Freeman 1989). These stars are particularly useful as they give a fair representation of the underlying stellar distribution (*cf.* e.g. Ibata & Gilmore 1995a). They have high intrinsic luminosity and well-behaved spectral features whose differences can be interpreted in terms of changes in temperature, abundance and surface gravity. However, local, intrinsically faint K dwarfs can contaminate these samples considerably. Fortunately, the sensitivity of absorption lines to the surface gravity of these stars allows one to discriminate between K giants and K dwarfs: this may be performed visually, by comparison to a grid of standards (e.g., Kuijken & Gilmore 1989), or by minimizing a statistic constructed from the stellar spectra and a grid of synthetic standards (e.g., Cayrel *et al.* 1991a, 1991b).

A number of alternative methods based on real stellar templates have been used for spectral classification including: Artificial Neural Networks (e.g., von Hippel *et al.* 1994); minimum distance methods and assorted methods based on cross-correlation (e.g., Kurtz 1984). Neural networks can offer a very sophisticated non-linear combination of input parameters and can be thought of as a variant of non-linear least squares minimization closely tied to a Bayesian classification scheme. While cross-correlation and the closely related (weighted) minimum distance methods are straightforward variants of least-squares fitting to standard templates. In this note we demonstrate the use of a robust optimal linear discrimination scheme based on a variant of Principal Components Analysis.

The data-set that is examined below was obtained with the AUTOFIB multi-fibers spectrograph at the Anglo Australian Telescope (AAT) with the aim of investigating the

kinematic and abundance structure of both the inner Milky Way (Ibata & Gilmore 1995a, 1995b), and the Sagittarius dwarf galaxy (Ibata, Gilmore & Irwin 1994). Though this instrument was efficient in gathering large samples of spectroscopic data, the resulting spectra cannot be directly compared to flux-calibrated spectra, because the spectrograph induces large, low-frequency variations in the shape of the spectra over wavelength ranges of width typically $\approx 200\text{\AA}$. This meant that the giant-dwarf discrimination technique of Carrel *et al.* (1991) could not be applied to the AUTOFIB data without considerable recalibration.

Ibata & Gilmore (1995a) therefore initially classified their ≈ 3000 spectra visually, following the prescription detailed in Kuijken & Gilmore (1989). However, it was clearly desirable to design an automated algorithm that is repeatable, that classifies stars to lower signal to noise than is possible visually, and that allows an estimate of the certainty of the classification to be made.

2. Visual Dwarf – Giant Classification for K stars

The survey-star spectra were first compared empirically to a grid of K giant and K dwarf standards. The standard spectra were observed by Kuijken & Gilmore (1989) and Ibata & Gilmore (1995a), again with the AUTOFIB fibers system. Standards at several $(B - V)_0$ are presented in Figure 1; a list of these stars is given in Table 1. The field dwarfs and metal poor dwarfs (subdwarfs) are from Bessel & Wickramasinghe (1979) and Rodgers & Eggen (1974), the metal rich dwarfs (Hyades dwarfs) are from Pels *et al.* (1975) and Upgren & Weiss (1977), while the giants are from Yoss *et al.* (1981), Friel (1986) and Faber *et al.* (1985). The most striking features in these spectra are the three Mg‘b’ lines at (5167, 5173 and 5184 \AA) and the MgH band at 5211 \AA (which also belongs to the Mg‘b’ feature). The other prominent lines are mostly TiO, Fe I and Fe II. Several properties of

K star atmospheres can be seen in the grid. In dwarfs, the prominent MgH band (5211 Å) is seen after $(B - V)_0 \gtrsim 1.05$, while in giants it appears only after $(B - V)_0 \gtrsim 1.25$. Fe lines are weaker even in super-metal-rich giants (*cf.* Table 1) than in Hyades dwarfs of the same color. For those stars with $(B - V)_0 > 1.1$, the wide Mg‘b’ absorption band (a wide dip stretching $5050\text{Å} \lesssim \lambda \lesssim 5200$) is strong in dwarfs, but is weak until $(B - V)_0 \approx 1.3$ in giants.

Cayrel *et al.* (1991) calculate synthetic spectra to find the surface gravity dependence of a K star spectrum in the wavelength range 4800 to 5300Å at fixed effective temperature and metallicity. In this situation they show that dwarfs display much stronger Mg, Fe and MgH lines than giants (because giants have lower surface gravity atmospheres and hence lower opacities). Cayrel *et al.* also calculate the metallicity dependence at constant surface gravity and effective temperature — as would be expected, higher metallicity increases the depth of the Mg and Fe lines and the MgH band (except for saturated Mg lines in metal poor dwarfs). Their results show clearly that the Mg‘b’ triplet and MgH band are more sensitive to gravity than to metallicity for stars of $[\text{Fe}/\text{H}] \gtrsim -1.25$, and that these lines can be as weak in metal poor dwarfs as they are in giants. Fortunately, along the lines of sight to these survey stars, starcount galaxy models predict a negligible contribution ($< 0.01\%$) of metal poor dwarfs (foreground halo stars) in the samples (Ibata 1994).

K giants and K dwarfs were in this way visually classified by comparison to the standards in Figure 1. The spectra were also binned into four groups, a subjective ranking of the certainty of the classification. The giant-dwarf classification was deemed to be satisfactory for high S/N spectra, but was clearly unsatisfactory on noisy spectra (judging from repeated attempts at classification), especially on the bluer end of the selection range ($(B - V)_0 \lesssim 1.0$).

3. Technique

Below, we first remind the reader of the standard PCA technique, and then describe the variant of this method which was successfully used to discriminate between K giants and K dwarfs.

To begin with, the spectra to be analyzed are shifted into their rest frames and binned linearly over a fixed wavelength range (4800-5500 Å) into a fixed number of bins N (500). Each spectrum can thus be represented as a point in the N -dimensional vector space of all possible (similarly binned) spectra.

As an example, consider the set of n_d standard dwarf spectra. This set can be represented as a cloud of n_d points in the above vector space. The aim of the standard PCA classification scheme is to concentrate the information in the n_d N -dimensional points into a set of q ($q < n_d$) orthogonal N -dimensional vectors which are able to describe “dwarf-ness” to good approximation (in a least squares sense). The largest of these vectors \mathbf{a}_1 is the direction along which the cloud of dwarf stars is most elongated, that is, the direction of a least squares line fit to the dwarf points that passes through the mean point (mean spectrum). This is the first order least squares description of the data. The variation of spectra in the direction \mathbf{a}_1 is the greatest in the data set, so it is removed by collapsing the cloud of points along \mathbf{a}_1 to give a new data-set of dimension $N - 1$. The second order least squares description \mathbf{a}_2 is calculated from this new data set in the same way as \mathbf{a}_1 was from the original set. This process is iterated so that the i th principal component is calculated from a data-set formed by successively collapsing the original data-set along the 1st to the $(i - 1)$ th principal component directions. The maximum number q_{max} of such vectors that can be found is either N (there are only N dimensions to collapse the data-set into) or n_d (when all points lie exactly along the $(q_{max} = n_d)$ th principal component). If dwarf star spectra have regular patterns, the cloud of points in the vector space will be localized, so

we expect to be able to account for most of the variance in the sample with a small number of principal components and the aim of the operation will have been fulfilled.

It can easily be shown (e.g., Francis 1991) that this process is equivalent to finding the eigenvectors corresponding to the largest eigenvalues of the matrix

$$C = \sum_i (\mathbf{x}_k)(\mathbf{x}_k)^H, \quad (1)$$

where H denotes Hermitian conjugate, and \mathbf{x}_k is the k th sample vector.

The problem that needs to be addressed however, is how to discriminate between classes of spectra (or clouds of points in the vector space of possible spectra). The variant of PCA employed here does not deconstruct a single set of spectra (cloud of points) as above, but instead deconstructs the set of difference vectors between points of different classes (again in a least squares sense) (see e.g., Ullman 1973). We will denote $\mathbf{x}_k^{(\mu)}$ as the k th sample vector of class μ . Since the mean spectrum $\bar{\mathbf{x}}$ contains no discriminatory information, we first subtract $\bar{\mathbf{x}}$ from all the $\mathbf{x}_k^{(\mu)}$: this does not affect discrimination and avoids the problem of the mean spectrum dominating the covariance matrix (Equation 10 below) which can make the eigenvector equation (Equation 9) unsuitable for solution with simple numerical algorithms.

Define a linear transformation A , such that

$$\mathbf{y}_k^{(\mu)} = A^H \mathbf{x}_k^{(\mu)}, \quad (2)$$

where $\mathbf{y}_k^{(\mu)}$ is to be set up such that it contains the maximum amount of discriminatory information based on a least-mean-square representation of all the difference vectors between the sets. Let \mathbf{a}_i be the vector elements of the transformation matrix $A = (\mathbf{a}_1, \dots, \mathbf{a}_i, \dots, \mathbf{a}_M)$, where M is a fixed number of elements less than or equal to N . We therefore seek unit

vectors \mathbf{a}_i that maximize the quantity

$$S^2 = \sum_{\substack{k,l,\mu,\mu' \\ \mu \neq \mu'}} (\mathbf{y}_k^{(\mu)} - \mathbf{y}_l^{(\mu')})^2. \quad (3)$$

The requirement that the \mathbf{a}_i be unit vectors imposes the constraint $(\mathbf{a}_i)^H \mathbf{a}_i = 1$. Then, using Lagrange multipliers, we may write:

$$\frac{d}{d\mathbf{a}_i} \left[\sum_{\substack{k,l,\mu,\mu' \\ \mu \neq \mu'}} (\mathbf{y}_k^{(\mu)} - \mathbf{y}_l^{(\mu')})^H (\mathbf{y}_k^{(\mu)} - \mathbf{y}_l^{(\mu')}) - \lambda_i \mathbf{a}_i^H \mathbf{a}_i \right] = 0, \quad (4)$$

where λ_i is the Lagrange multiplier for \mathbf{a}_i . Substituting for $\mathbf{y}_k^{(\mu)}$ from Equation 2:

$$\frac{d}{d\mathbf{a}_i} \left[\sum_{\substack{k,l,\mu,\mu' \\ \mu \neq \mu'}} (\mathbf{x}_k^{(\mu)} - \mathbf{x}_l^{(\mu')})^H (A A^H) (\mathbf{x}_k^{(\mu)} - \mathbf{x}_l^{(\mu')}) - \lambda_i \mathbf{a}_i^H \mathbf{a}_i \right] = 0. \quad (5)$$

Putting $\mathbf{b}_{kl}^{(\mu\mu')} = (\mathbf{x}_k^{(\mu)} - \mathbf{x}_l^{(\mu')})$:

$$\frac{d}{d\mathbf{a}_i} \left[\sum_{\substack{k,l,\mu,\mu' \\ \mu \neq \mu'}} (\mathbf{b}_{kl}^{(\mu\mu')})^H A A^H \mathbf{b}_{kl}^{(\mu\mu')} - \lambda_i \mathbf{a}_i^H \mathbf{a}_i \right] = 0. \quad (6)$$

$$\sum_{\substack{k,l,\mu,\mu' \\ \mu \neq \mu'}} \frac{d}{d\mathbf{a}_i} \left[(\mathbf{a}_1 \cdot \mathbf{b}_{kl}^{(\mu\mu')}, \dots, \mathbf{a}_i \cdot \mathbf{b}_{kl}^{(\mu\mu')}, \dots, \mathbf{a}_n \cdot \mathbf{b}_{kl}^{(\mu\mu')}) \begin{pmatrix} \mathbf{a}_1 \cdot \mathbf{b}_{kl}^{(\mu\mu')} \\ \vdots \\ \mathbf{a}_i \cdot \mathbf{b}_{kl}^{(\mu\mu')} \\ \vdots \\ \mathbf{a}_n \cdot \mathbf{b}_{kl}^{(\mu\mu')} \end{pmatrix} - \lambda_i \mathbf{a}_i^H \mathbf{a}_i \right] = 0. \quad (7)$$

Differentiating:

$$2 \left[\sum_{\substack{k,l,\mu,\mu' \\ \mu \neq \mu'}} \mathbf{b}_{kl}^{(\mu\mu')} (\mathbf{b}_{kl}^{(\mu\mu')})^H - \lambda_i \mathbf{I} \right] \mathbf{a}_i = 0, \quad (8)$$

or:

$$[\mathbf{C} - \lambda_i \mathbf{I}] \mathbf{a}_i = 0. \quad (9)$$

Therefore the \mathbf{a}_i are eigenvectors of the Hermitian matrix \mathbf{C} :

$$\mathbf{C} = \sum_{\substack{k,l,\mu,\mu' \\ \mu \neq \mu'}} (\mathbf{x}_k^{(\mu)} - \mathbf{x}_l^{(\mu')}) (\mathbf{x}_k^{(\mu)} - \mathbf{x}_l^{(\mu')})^H, \quad (10)$$

which is simply the covariance matrix of the difference vectors. The eigenvectors $\mathbf{a}_1, \dots, \mathbf{a}_i, \dots, \mathbf{a}_M$ of the covariance matrix define the linear transformation A (Equation 2 above).

Substituting Equation 9 into Equation 3 and using the orthogonality property of the eigenvectors, we find

$$S^2 = \sum_{i=1}^m \lambda_i, \quad (11)$$

where m is the no. of eigenvectors used. Clearly the larger the eigenvector the larger the discriminating power of the corresponding eigenvector. Therefore, the M eigenvectors with the largest eigenvalues give the best M -dimensional linear discrimination between classes μ and μ' .

4. Results

We first find the mean spectrum of the 48 standard stars displayed in Figure 1. The covariance matrix C (Equation 10) is formed using the mean-corrected standard star spectra. The eigenvectors \mathbf{a}_i and related eigenvalues λ_i of the covariance matrix C are then calculated. As explained above, the eigenvectors corresponding to the largest eigenvalues are those which contain the greatest amount of discriminatory information: the ten largest eigenvalues are given in Table 2. From the table we see that the first order discriminating vector (that with the largest eigenvalue) accounts for a large fraction — $\approx 50\%$ — of the total discrimination, with the next nine contributing only a further $\approx 35\%$. We therefore investigate whether the first order eigenvector is sufficient to allow distinction between K dwarfs and K giants. This eigenvector is shown in Figure 2: several spectral features of K stars are visible, notably the Mg‘b’ feature, the MgH band at 5205\AA and some prominent Fe lines.

For each star spectrum \mathbf{x} that is to be classified, a coefficient $c = (\mathbf{x} - \bar{\mathbf{s}}) \cdot \mathbf{e}$ is calculated from the eigenvector \mathbf{e} (shown in Figure 2) and the average standard star spectrum $\bar{\mathbf{s}}$. Figure 3 shows the relation between $(B - V)_0$ and c calculated for the standard stars; the ‘stars’ in the diagram represent the giants in the sample of standards, the large dots represent dwarf stars and the small dots represent subdwarfs. Superimposed is a straight line drawn by eye marking the boundary between giants and dwarfs. For $(B - V)_0 > 1.1$, the classification scheme appears to work well. For $(B - V) \lesssim 1.0$, the classification is less clear cut (but it is also very difficult to classify these hotter stars visually — *cf.* Section 2).

Figure 4 shows the same plot for the survey stars, where the $(B - V)_0$ values have been taken from the calibrated APM photometry (*cf.* Ibata & Gilmore 1995a).

We now estimate the accuracy of this classification scheme. The effect of photon noise on classification is investigated by degrading the standard star spectra using a Poisson random number generator by Press *et al.* (1986). We find an *rms* error in the coefficient c of ≈ 10 when the signal to noise is degraded to $S/N \approx 5$ (for the standard stars, c takes values $-100 \lesssim c \lesssim 100$). A very much larger source of error in the classification of survey stars arises simply from the *rms* color error $(B - V) \approx 0.18$ of these data (Ibata & Gilmore 1995a). Assuming that each point in Figure 4 has a probability density that is a Gaussian distribution with $\sigma = 0.18$ along the $(B - V)$ direction, we find that $\approx 15\%$ of giants and $\approx 25\%$ of dwarfs are on average misidentified.

Comparing the results of automated classification to that performed visually (*cf.* Section 2), we find that $\approx 11\%$ of all dwarfs classified visually are classified differently by the PCA algorithm ($\approx 5\%$ for high signal to noise spectra with $(B - V) > 1.1$), while $\approx 13\%$ of giants classified visually are classified differently by the algorithm ($\approx 8\%$ for high signal to noise spectra with $(B - V) > 1.1$). (By high signal to noise spectra we mean approximately the quarter of the survey sample of which we were most confident of the

visual classification). We cannot easily quantify the relative precision between the automatic and visual techniques since it is non-trivial to organize a controlled experiment on humans. However, in the few cases where an inter- and intra-comparison between classification by human experts and an automated algorithm has been carried out for related problems (e.g., Naim *et al.* 1995, Lahav *et al.* 1995 for galaxy morphology classification), the scatter between different human experts was found to be non-negligible and indeed comparable to the error from the automatic technique. What is clear from our tests is that repeated human attempts at visual classification of low signal to noise ($S/N \approx 10$) spectra are much less reliable than the machine based approach (although again it is difficult to quantify this statement).

5. Conclusions

We discussed a variant of the Principal Component Analysis technique, which is designed to discriminate between classes of objects. This technique provides the best possible linear discrimination. It is well suited to astronomical problems involving the discrimination of spectra. We show that it is very simple to implement this technique on the problem of distinguishing K dwarfs from K giants using spectra sampled in the wavelength range 4800 to 5300Å at $\approx 1.5\text{Å}$ resolution. In principle, with very accurate $(B - V)_0$ photometry, and with very high signal to noise spectra (say, $S/N \gtrsim 30$) it is possible to discriminate visually between K giants and K dwarfs to high accuracy. However, the K star sample investigated above had poor photometry ($\delta(B - V)_0 \approx 0.2$), and many spectra had $S/N \lesssim 10$ (for which repeated attempts at visual discrimination gave different results). The numerical algorithm developed is able to reproduce visual discrimination of the highest signal to noise spectra ($S/N \gtrsim 20$) to approximately 90 – 95% (and helped to pick out stars which, with hindsight, had been obviously misclassified). According to numerical

experiments, in which standard star spectra had their signal to noise ratio degraded artificially to $S/N \approx 5$ (about the lowest S/N spectrum obtained), the algorithm works well with poor quality spectra. The machine discrimination is reliable (the discrimination criteria remain fixed) and is much more accurate than visual discrimination on low signal to noise spectra.

REFERENCES

- Burstein, D. and Heiles, C. 1982, *AJ*, 87, 1165
- Cayrel, R., Perrin, M., Barbuy, B. and Buser, R. 1991, *A&A*, 247, 108
- Cayrel, R., Perrin, M., Buser, R., Barbuy, B. and Coupry, M. 1991, *A&A*, 247, 122
- Bessel, M. and Wickramasinghe, D. 1979, *ApJ*, 227, 232
- Faber, S., Friel, E., Burstein, and D., Gaskell C. 1985, *ApJS*, 57, 711
- Francis, P. 1991, Ph.D. Thesis, Cambridge University
- Friel, E. 1986, PhD Thesis, University of California
- von Hippel, T., Storrie-Lombardi, L.J., Storrie-Lombardi, M.C. and Irwin, M.J. 1994, *MNRAS*, 269, 97
- Ibata, R. 1991, Ph.D. Thesis, Cambridge University
- Ibata, R., Gilmore, G., and Irwin, M. 1994, *Nature*, 370, 194.
- Ibata, R. and Gilmore, G. 1995a, *MNRAS*, 275, 591
- Ibata, R. and Gilmore, G. 1995b, *MNRAS*, 275, 605
- Kuijken, K. and Gilmore, G. 1989, *MNRAS*, 239, 605
- Kurtz, M.J. 1984, in *The MK Process and Stellar Classification*, Ed. Garrison, R.F., pp 136-152, David Dunlap Observatory, Toronto, Canada.
- Lahav, O., Naim, A., Buta, R., Corwin, H., de Vaucouleurs, G., Dressler, A., Huchra, J., van den Bergh, S., Raychaudhury, S., Sodre, L. and Storrie-Lombardi, M. 1995, *Science*, 267, 859L
- Lewis, J. and Freeman, K. 1989, *AJ*, 97, 139

- Naim, A., Lahav, O., Buta, R., Corwin, H., de Vaucouleurs, G., Dressler, A., Huchra, J., van den Bergh, S., Raychaudhury, S., Sodre, L. and Storrie-Lombardi, M. 1995, MNRAS, 274, 1107
- Pels, G., Oort, J. and Pels-Kluyver, H. 1975, A&A, 43, 423
- Press, W., Flannery, B., Teukolsky, S. and Vetterling, W. 1986, *Numerical Recipes*, Cambridge
- Rich, R. 1990, ApJ, 362, 604
- Rich, R. 1988, AJ, 95, 828
- Rodgers, A. and Eggen, O. 1974, PASP, 86, 742
- Ullman, J. 1973, *Pattern Recognition Techniques*, London, Butterworths
- Ungren, A. and Weiss, E. 1977, AJ, 82, 978
- Yoss, K., Karman, R. and Hartkopf, W. 1981, AJ, 86, 36

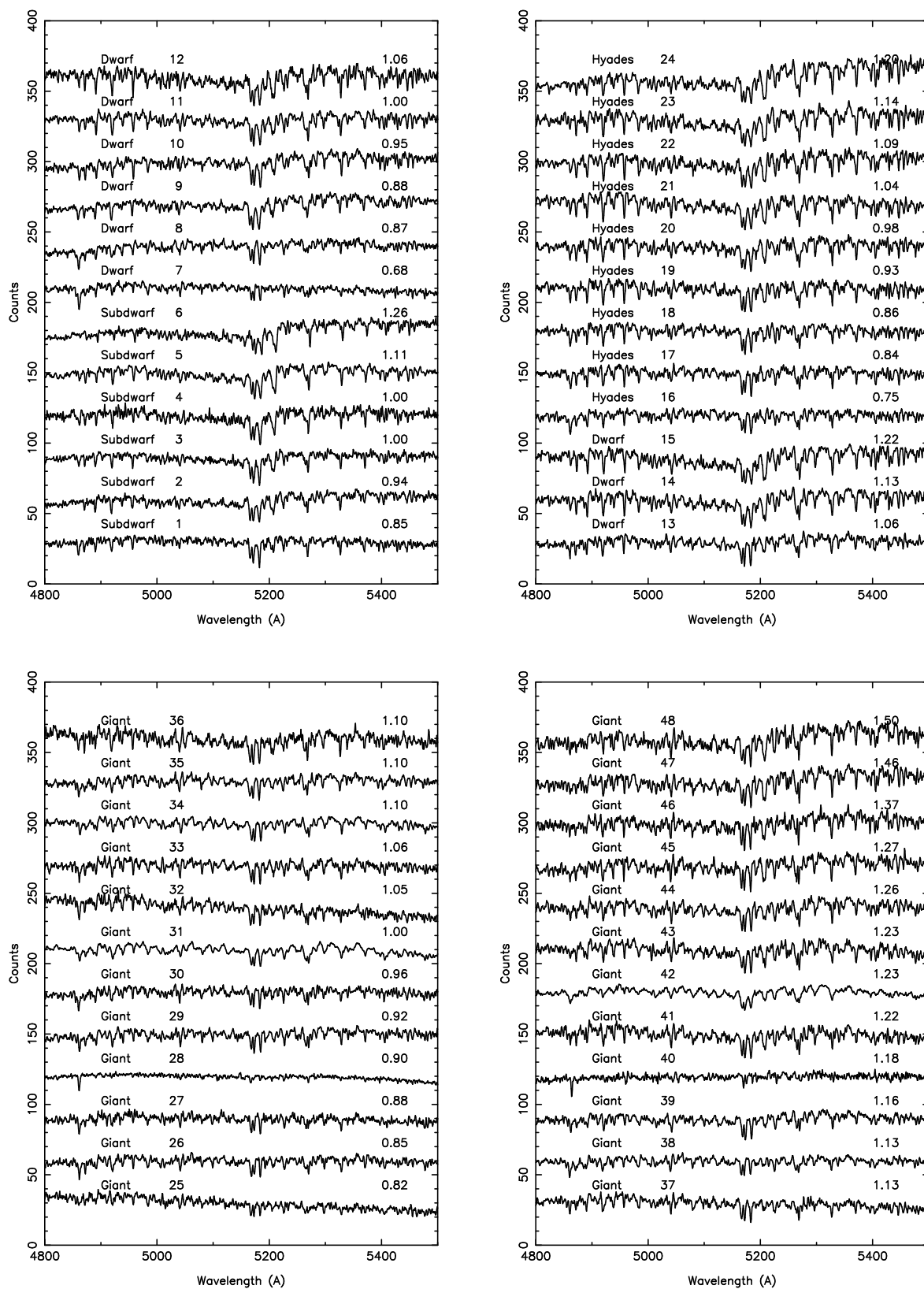


Fig. 1.— The grid of spectral standard stars. Each star is labeled with a classification (subdwarf dwarf Hyades star giant) with an identification number (1 – 48, corresponding

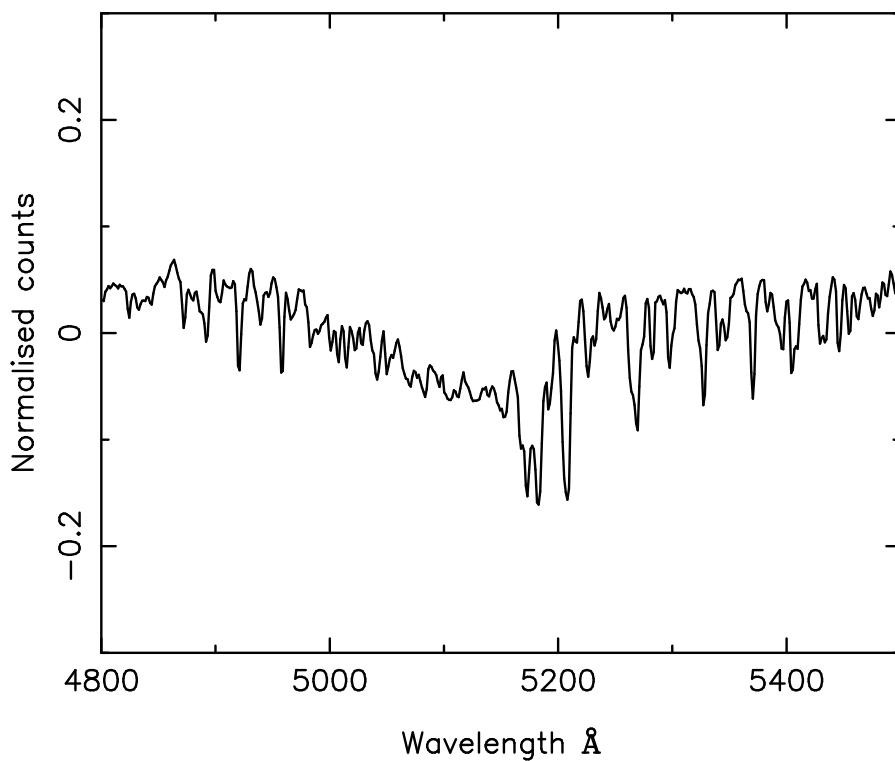


Fig. 2.— The most discriminating vector between K dwarfs and K giants (that corresponding to λ_1 in Table 2). The dot product of this vector with a vector formed by the subtraction

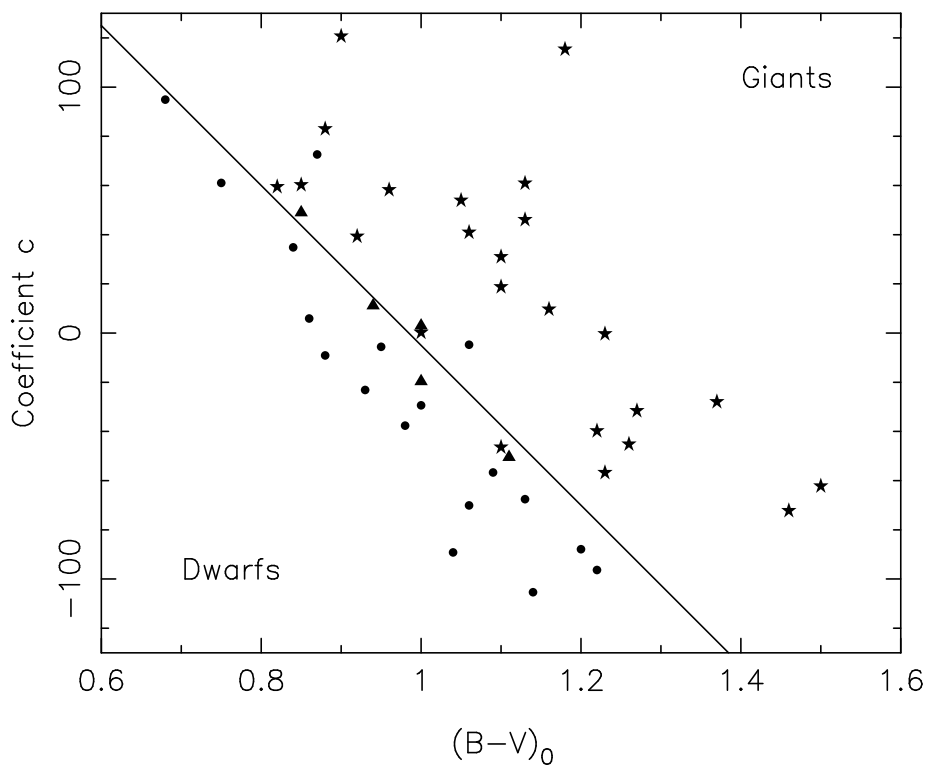


Fig. 3.— The color dependence of the coefficient c (defined in the text) with $(B - V)_0$ for the standards shown in Figure 1. The ‘stars’ in the diagram are giants, the ‘filled circles’ are

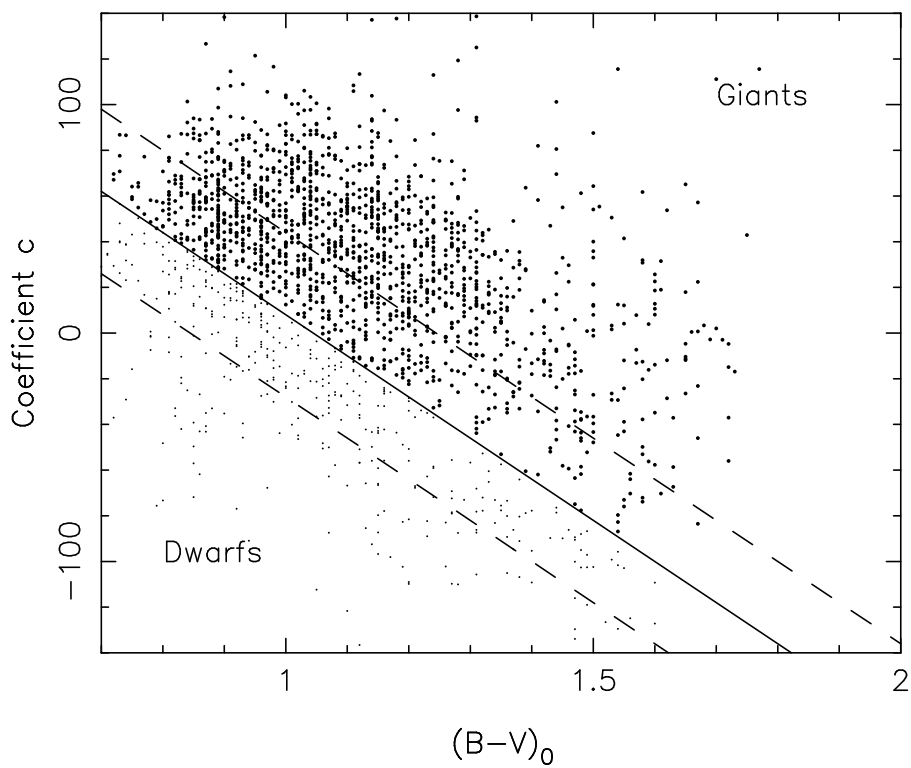


Fig. 4.— Spectral classification of survey stars. Given the giant-dwarf boundary shown in Figure 3, the survey stars have been classified into ‘large dots’-giants and ‘dots’-dwarfs. The

Table 1. The grid of standard stars

No.	Class	B – V	star	No.	Class	B – V	star	[Fe/H]
1	subdwarf	0.85	LFT 1756	25	giant	0.82	HD 191179	
2	subdwarf	0.94	BD–0°4234	26	giant	0.85	HD 201195	
3	subdwarf	1.00	LFT 466	27	giant	0.88	HD 203066	
4	subdwarf	1.00	G 155-35	28	giant	0.90	HR 5270	-2.60
5	subdwarf	1.11	LFT 100	29	giant	0.92	HD 171391	
6	subdwarf	1.26	LFT 1668	30	giant	0.96	HD 192246	
7	dwarf	0.68	HR 72	31	giant	1.00	HR 3994	0.22
8	dwarf	0.87	HR 7703	32	giant	1.05	HD 202978	
9	dwarf	0.88	HR 487	33	giant	1.06	HD 157457	
10	dwarf	0.95	HR+21°3245	34	giant	1.10	HR 4287	-0.06
11	dwarf	1.00	HR 8382	35	giant	1.10	HR 8841	-0.13
12	dwarf	1.06	HR 8387	36	giant	1.10	HR 8924	0.55
13	dwarf	1.06	BD+10°3665	38	giant	1.13	HR 7430	-0.70
14	dwarf	1.13	BD+22°3406	37	giant	1.13	HD 211475	
15	dwarf	1.22	BD+6°4741	39	giant	1.16	HD 107328	-0.47
16	Hyades	0.75	vB 69	40	giant	1.18	HD 110184	-2.50
17	Hyades	0.84	Pels 50	41	giant	1.22	HD 202168	
18	Hyades	0.86	Pels 56	42	giant	1.23	HR 5340	-0.42
19	Hyades	0.93	Pels 52	43	giant	1.23	HR 5370	0.31
20	Hyades	0.98	Pels 63	44	giant	1.26	HR 5582	0.42
21	Hyades	1.04	Pels 39	45	giant	1.27	HD 201875	
22	Hyades	1.09	Pels 51	46	giant	1.37	HR 0489	-0.11
23	Hyades	1.14	Pels 49	47	giant	1.46	HR 6136	0.35
24	Hyades	1.20	Pels 65	48	giant	1.50	HR 0224	-0.07

Table 2. The ten largest eigenvalues of the covariance matrix of standard stars.

No.	λ	% of trace	cum. % of trace
1	7027827.5	50.145	50.145
2	1836905.6	13.107	63.252
3	1277226.4	9.113	72.365
4	606478.0	4.327	76.692
5	295777.4	2.110	78.803
6	251045.7	1.791	80.594
7	207668.2	1.482	82.076
8	159497.0	1.138	83.214
9	149020.3	1.063	84.277
10	146001.9	1.042	85.319

TABLE 1. The grid of standard stars

No.	Class	B – V	star	No.	Class	B – V	star	[Fe/H]
1	subdwarf	0.85	LFT 1756	25	giant	0.82	HD 191179	
2	subdwarf	0.94	BD–0°4234	26	giant	0.85	HD 201195	
3	subdwarf	1.00	LFT 466	27	giant	0.88	HD 203066	
4	subdwarf	1.00	G 155-35	28	giant	0.90	HR 5270	-2.60
5	subdwarf	1.11	LFT 100	29	giant	0.92	HD 171391	
6	subdwarf	1.26	LFT 1668	30	giant	0.96	HD 192246	
7	dwarf	0.68	HR 72	31	giant	1.00	HR 3994	0.22
8	dwarf	0.87	HR 7703	32	giant	1.05	HD 202978	
9	dwarf	0.88	HR 487	33	giant	1.06	HD 157457	
10	dwarf	0.95	HR+21°3245	34	giant	1.10	HR 4287	-0.06
11	dwarf	1.00	HR 8382	35	giant	1.10	HR 8841	-0.13
12	dwarf	1.06	HR 8387	36	giant	1.10	HR 8924	0.55
13	dwarf	1.06	BD+10°3665	38	giant	1.13	HR 7430	-0.70
14	dwarf	1.13	BD+22°3406	37	giant	1.13	HD 211475	
15	dwarf	1.22	BD+6°4741	39	giant	1.16	HD 107328	-0.47
16	Hyades	0.75	vB 69	40	giant	1.18	HD 110184	-2.50
17	Hyades	0.84	Pels 50	41	giant	1.22	HD 202168	
18	Hyades	0.86	Pels 56	42	giant	1.23	HR 5340	-0.42
19	Hyades	0.93	Pels 52	43	giant	1.23	HR 5370	0.31
20	Hyades	0.98	Pels 63	44	giant	1.26	HR 5582	0.42
21	Hyades	1.04	Pels 39	45	giant	1.27	HD 201875	
22	Hyades	1.09	Pels 51	46	giant	1.37	HR 0489	-0.11
23	Hyades	1.14	Pels 49	47	giant	1.46	HR 6136	0.35
24	Hyades	1.20	Pels 65	48	giant	1.50	HR 0224	-0.07

TABLE 1. The ten largest eigenvalues of the covariance matrix of standard stars.

No.	λ	% of trace	cum. % of trace
1	7027827.5	50.145	50.145
2	1836905.6	13.107	63.252
3	1277226.4	9.113	72.365
4	606478.0	4.327	76.692
5	295777.4	2.110	78.803
6	251045.7	1.791	80.594
7	207668.2	1.482	82.076
8	159497.0	1.138	83.214
9	149020.3	1.063	84.277
10	146001.9	1.042	85.319